ELSEVIER

Journal of Structural Geology 27 (2005) 627–644

JOURNAL OF STRUCTURAL GEOLOGY

www.elsevier.com/locate/jsg

Control of the geometry of precursor brittle structures on the type of ductile shear zone in the Adamello tonalites, Southern Alps (Italy)

Giorgio Pennacchioni*

[a]*Dipartimento di Geologia, Paleontologia e Geofisica, University of Padova, Italy*
[b]*CNR-Istituto di Geoscienze e Georisorse (Sezione di Padova), Italy*

Received 7 July 2004; received in revised form 10 November 2004; accepted 13 November 2004
Available online 5 March 2005

Abstract

Amphibolite facies ductile shear zones developed during the immediate post-intrusive cooling history of the Adamello tonalites (Southern Alps, Italy). Shear zones include: (i) thin (a few mm's thick) fault-like shear zones that accommodate shear strain values up to several 100's (the dominant type); (ii) mylonitic horizons (dm's thick) in sharp contact with the undeformed wall rock; (iii) continuous shear zones with sigmoidal-shaped S or composite S–C′ foliations. A transition between the different types occurs along strike over short distances. Discontinuous shear zones are also localized on pegmatite dykes and quartz veins, and both (i) and (ii) are discontinuously outlined by quartz layers. Detailed surface mapping reveals that most fault-like shear zones are arranged en-échelon, mainly forming contractional steps. Markers crosscut by shear zones allow the displacement to be measured at several positions along shear zones and this reveals very steep displacement gradients close to the shear zone tips. Differential displacement is mainly accommodated at contractional steps by the development of foliated domains. Geochemical analyses of major and trace elements show that there is no compositional change along strain gradients. The overall features are consistent with nucleation of shear zones on former sets of en-échelon joints, in many cases intruded by pegmatite dykes or filled with quartz. Reactivation of joints produced strongly localized shear zones, whereas broader foliated zones evolved from the contractional jogs between adjacent stepped joint terminations during progressive shearing. These jogs were progressively involved in the accommodation of shear displacement and overall shear zone development.

Keywords: Ductile shear zones; Brittle precursor; Deformation of intrusive rocks; Reactivated joints

1. Introduction

In both material science and geological literature, dynamic material instability is often invoked as a main cause for strain localization in discrete shear zones (Hobbs et al., 1990). In this case, it is the constitutive behaviour of the material itself that is the intrinsic reason for instability. In non-dilatant materials, localization is promoted by power-law rheology and, especially, by strain softening behaviour (e.g. Mancktelow, 2002). However, localization may also arise from purely geometric instabilities such as the existence of compositional heterogeneities (e.g. Christiansen and Pollard, 1997) and of former (precursory or pre-existing in the sense of Crider and Peacock (2004)) brittle discontinuities (i.e. fractures, often filled with veins). Strongly localized shear zones associated with a brittle-to-ductile deformation sequence have been described in several granitoid massifs (Segall and Pollard, 1983; Segall and Simpson, 1986; Tobish et al., 1991; Tourigny and Tremblay, 1997; Guermani and Pennacchioni, 1998; Takagi et al., 2000; Mancktelow and Pennacchioni, 2005) or coarse-grained non-foliated protoliths under different metamorphic conditions (Austrheim, 1987; Pennacchioni, 1996). Therefore, localization on brittle precursor structures may be a relatively common mode of nucleation/localization of strain in relatively coarse-grained and isotropic rocks.

In some cases, localization of ductile shear on former fractures has been related to the infiltration of aqueous fluids triggering different softening effects (e.g. Austrheim, 1987; Boundy et al., 1992; Pennacchioni, 1996). Under greenschist facies metamorphic conditions, localization within granitoids is often promoted by feldspar alteration to

* Tel.: +39-49-8273938; fax: +39-49-8272070
E-mail address: giorgio.pennacchioni@unipd.it.

0191-8141/$ - see front matter © 2005 Elsevier Ltd. All rights reserved.
doi:10.1016/j.jsg.2004.11.008

mica-rich fine-grained aggregates along fractures (e.g. Tourigny and Tremblay, 1997; Guermani and Pennacchioni, 1998). Ductile reuse of brittle discontinuities is often reflected in the discontinuous geometry of shear zones (Guermani and Pennacchioni, 1998). However, there is still little understanding on how (i) the mesoscale spatial arrangement of pre-existing fractures and the degree of fluid–rock interaction along them affect the geometry of the overprinting ductile shear zones and (ii) the mylonitic fabric progressively develops at different locations in the fracture network. Some detailed mesoscale analysis has been carried out in the Sierra Nevada granites (Bürgmann and Pollard, 1992, 1994; Christiansen and Pollard, 1997) recording a brittle-to-ductile history. In these granites, ductile shear occurred under fluid-present conditions, which resulted in the development of veins in extensional domains at fracture tips (i.e. the symmetrical opposite of the foliated domains in contractional quadrants observed in this study). Away from the tips, precursor fractures (joints) were reactivated as discrete, highly localized shear zones.

This paper describes examples of amphibolite facies ductile shear zones within tonalites of the Adamello massif, northern Italy. The observed features show many similarities to those of the Sierrean granites, but there are also important differences. Rather exceptional exposure conditions on glacier-polished outcrops and the incipient degree of ductile overprint allow shear zone nucleation on former joint sets to be carefully documented. It also allows a detailed study of the control exerted by the pre-existing geometric arrangement of brittle precursors on the developing ductile fabric and on the shear zone geometry, under conditions that were apparently water-deficient.

2. Geological setting

The Adamello batholith is the largest (670 km^2) of the Periadriatic Tertiary plutons in the Alps. It intruded into a stack of south-vergent thrusts forming the Southern Alps, which involved both pre-Alpine basement and Mesozoic cover rocks. It occurs close to the intersection between two major Alpine lineaments: the Tonale and Giudicarie Faults. The Adamello consists of four main, dominantly tonalitic, intrusive bodies, which were emplaced sequentially from south to north in the time range 42–30 Ma (Bianchi et al., 1970) (Fig. 1). Each intrusive body cooled rapidly after emplacement to brittle–ductile transition conditions ($T<$ 250–300 °C), as inferred from the overlap in the different radiometric mineral ages within each single intrusion (U–Pb on zircons, Rb–Sr and K–Ar on biotite and muscovite, Ar–Ar dating of pseudotachylytes: Del Moro et al., 1983; Hansmann and Oberli, 1991; Viola et al., 2003; Stipp et al., 2004; Pennacchioni et al., submitted). The rapid cooling reflects the shallow depth of intrusion (9–11 km), as estimated from the mineral paragenesis in the metamorphic

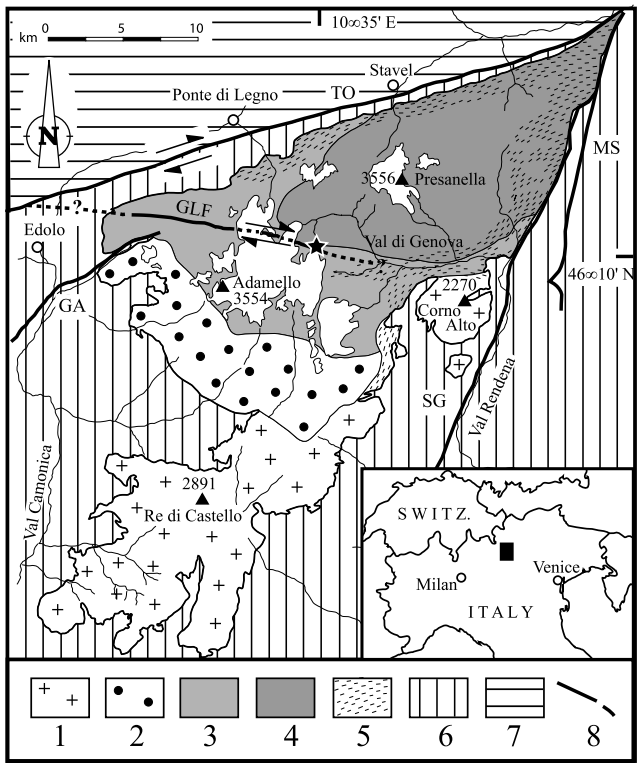

Fig. 1. Geological sketch map of the Adamello pluton (modified from Bianchi et al. (1970)). (1)–(5) Composite Adamello batholith: (1) Re di Castello intrusion (42–40 Ma); (2) Western Adamello intrusion (36–34 Ma); (3) Central Peaks and Avio intrusions (34–32 Ma); (4) Presanella intrusion (33–29 Ma); (5) foliated tonalites. (6) Basement and cover of the Southern Alps. (7) Austroalpine nappes. (8) Major tectonic lines: GA = Gallinera; GLF = Gole Larghe Fault; MS = Monte Sabion; SG = Southern Giudicarie; TO = Tonale. The black star indicates the location of the studied outcrop.

contact aureole (P = 0.25–0.3 GPa: Riklin, 1985; Werling, 1992).

In the Adamello, each single intrusion records a post-magmatic deformation evolution that can be referred to the cooling history of the specific intrusion. In the north-western part of the Adamello, within the tonalites of the Avio and Central Peaks intrusions, Pennacchioni et al. (submitted) recognized a sequence of structures, from older to younger: (i) joints, forming a pervasive composite network of different sets of conjugate planes, (ii) discrete amphibolite facies ductile shear zones, (iii) indurated cataclasites and pseudotachylytes concentrated along E–W-trending strike-slip faults, and (iv) late faults associated with pervasive zeolite-filled veining. The ductile shear zones must refer to the cooling history of the pluton as amphibolite facies conditions were never imposed on the pluton after it cooled.

3. Geometry of ductile shear zones: field description

The ductile shear zones described here are present within

the Avio tonalites in the outcrops at the front of the Lobbia Glacier, in the upper Genova Valley (see location in Fig. 1). In this area, ductile shear zones are frequent and occur in two main arrays of subparallel structures with orientations (here always given as dip direction and dip) of N80°–35° (shear zones$_1$) and N200°–80° (shear zones$_2$). Their orientation is identical to that of joints, which are pervasive throughout the Avio intrusion. Shear zones$_1$ are numerous, with spacing in the order of decimetres to a few meters. They have shallowly north-plunging stretching lineations (pitch $<30°$) and the sense of shear is sinistral. Shear zones$_2$ are less common. They have steeply plunging lineations (pitch $>45°$) but on flat outcrop planes the foliation geometry and marker displacement indicate a dextral component of shear. Kinematic indicators on *XZ* sections (i.e. parallel to lineation and orthogonal to foliation) of shear zones$_2$ record a normal top-to-south sense of movement.

The shear zones display various geometries: (i) continuous shear zones with sigmoidal-shaped S-type foliation (Fig. 2a), (ii) S–C′ mylonites (Fig. 2b), and (iii) discontinuous shear zones that include very localized types, with a thickness of only a few millimetres (Fig. 2c and d), and mylonitic horizons up to few decimetres in thickness, with a strong foliation parallel to the boundaries with the undeformed host tonalite (Fig. 2e). Transitions between the different types of shear zones occur over short distances along strike. It is also relatively common that S and S–C′ foliation patterns are developed asymmetrically on one or both sides of mylonitic horizons or sharp shear zones (Fig. 2b). S and S–C′ foliations are in turn locally bounded between paired subparallel sharp shear planes. The total thickness of shear zones rarely exceeds 1 m.

To elucidate the geometry of the shear zones and the spatial relationships between the different shear zone types, a glacier-polished outcrop (coordinates: N46°10′207″; E10°35′265″) was mapped in detail in the Lobbia area. Owing to the very recent glacier retreat, the outcrop is completely unweathered and provides exceptional exposures. An area of approximately 675 m^2 of smooth, gently sloping outcrop (the outcrop surface is nearly parallel to the stretching lineation of the mylonites) was mapped using a 1 m square grid marked off in 10 cm units, which allowed a precision of <1 cm in drawing. The map is shown in Fig. 3. It must be emphasized that the outcrop surface is not perfectly planar, which results in some distortion of structures in 2D map view. The studied outcrop is a few tens of meters south of the boundary of a major E–W-trending dextral strike-slip cataclastic fault zone (the Gole Larghe Fault: Di Toro and Pennacchioni, 2004; GLF in Fig. 1). This fault zone is outlined by horizons (mm's to dm's in thickness) of indurated cataclasites/pseudotachylytes and associated with a strong fracture-related alteration and veining (K-feldspar–epidote–chlorite-filled veins) of the host tonalites. However, this deformation and alteration phase affected the studied outcrop only very weakly or not at all.

The mapped area contains numerous subparallel sinistral shear zones$_1$ (striking ca. N–S: Fig. 4a), with a spacing in the range of <1 m to a few meters, rare dextral shear zones$_2$ (striking ca. E–W), aplitic dykes/schlieren layers (most in a set with dip direction and dip of N210°–50°, i.e. at a high angle to shear zones$_1$: Fig. 4b) and basic enclaves (with mean maximum elongation, determined by image analysis of the map, scattered around N103° and with a standard deviation of 28.5°). In the map and the following discussion, the individual shear zones and aplitic dykes/schlieren layers are identified by uppercase bold letters (**A**–**R**) and numbers (**1**–**23**), respectively. Shear zones with the same identifier letter but different indexes are coplanar shear zone segments or associated with en-échelon arrays (e.g. **E$_1$**, **E$_2$**). Many shear zones have one or both ends inside the mapped area and are slightly non-coplanar (separation is on the order of a few decimetres) with partly overlapping terminations. In fact, those shear zones with a larger separation are also arranged in an en-échelon manner (**A** vs. **B**–**C** and **O** vs. **P**). In most cases, the length of overlapping shear zone segments is in the same range as the separation.

Most ductile shear zones are extremely localized fault-like structures. They appear as sharp planes or thin horizons, a few millimetres in width, crosscutting undeformed tonalites. Macroscopically they closely resemble joints, which are pervasive within the whole intrusion, except that they accommodate relatively large displacements as recorded by marker offsets (Fig. 2c). Measured shear strain values range up to several 100's (e.g. in Fig. 3c the displacement of **15** across **A**, which is about 0.2 cm thick, is 50 cm corresponding to $\gamma = 250$, but shear strains up to ca. 750 were measured). Unlike joints, there is often a discernible structure within the fault-like shear zones: in close-up view or with a hand lens, a prominent foliation parallel to the shear zone boundaries is visible. In many cases, despite the large accommodated shear strain, long segments of these thin shear zones display sharp boundaries between the foliated material inside the shear zone and the host tonalite, with no foliation or drag of the displaced markers close to the shear zone boundary (Fig. 2c). In other cases, a weak foliation is present in the country rock close to fault-like shear zones. It is often developed asymmetrically with a different intensity and orientation on the two sides of the fault-like plane and may change in shape along the shear zone length over only short distances (Fig. 2d). Foliation has a geometry consistent with the sinistral sense of shear, but locally the acute angle that forms with the adjacent fault-like shear horizon exceeds 45°.

Veins and layers of milky quartz are common along and parallel to the shear zones (Fig. 5a). The thickest ones (up to 30 cm) are shown on the map of Fig. 3, but several shear zones are discontinuously decorated by a thin (a few mm's to cm's thick) quartz layer parallel to the shear zone plane. Quartz veins show tapering tips, extending into fault-like shear zones, or blunt terminations. They never display zoning features or fibrous crystal growth, and are massive

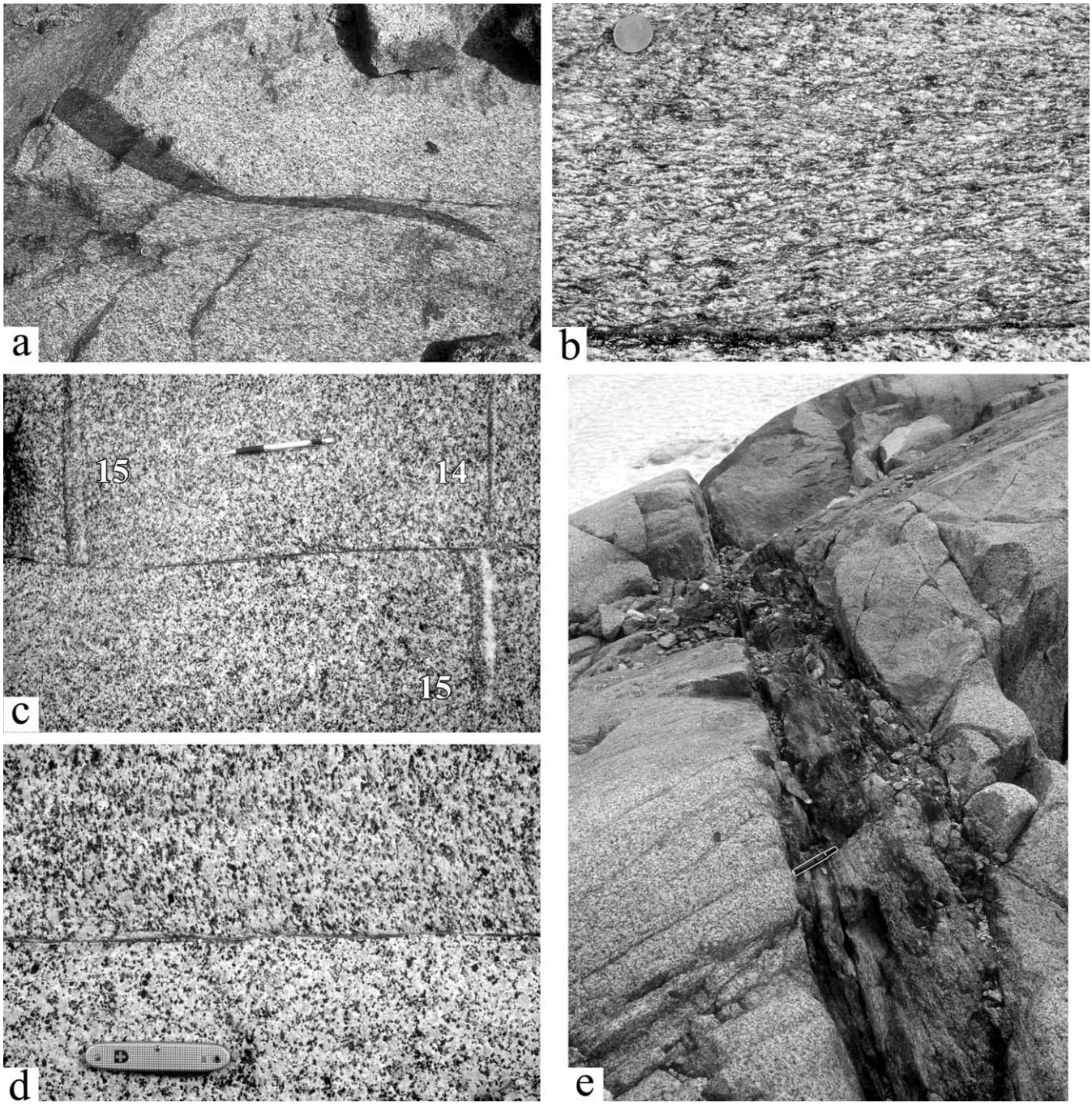

Fig. 2. Ductile shear zones in the Lobbia outcrops. (a) Sigmoidal-shaped basic enclave deformed across a continuous ductile shear zone$_1$. (b) S–C′ mylonite (shear zone$_1$); note the rather sharp ultramylonitic boundary in the lower part of the photo separating the S–C′ fabric from the foliated tonalite below. (c) Fault-like shear zone$_1$ (**D**) displacing aplites **14** and **15**; displacement of **15** is 50.5 cm and **D** is about 0.2 cm thick, which corresponds to a $\gamma = 250$; note the absence of any significant drag-like distortion of the aplitic dykes and the absence (or the very incipient local formation) of a foliation in the tonalite adjacent to the shear zone. (d) Fault-like shear zone$_1$ associated with a weak foliation in the host tonalite on one (upper) side. A small discontinuous quartz lens is visible along the left part of the shear zone. (e) Discontinuous ultramylonitic shear zone$_2$ with a sharp boundary to undeformed tonalite. Sense of shear is sinistral in (a)–(d) (shear zones$_1$); in (c) marker displacement (not visible in the photo) indicates a component of dextral shear on the flat outcrop surface (shear zones$_2$). Scale: coin (2.3 cm in diameter) in (a) and (b), pencil (14.5 cm long) in (c), Swiss knife (9.3 cm long) in (d) and felt-tipped pen (13.5 cm long), outlined with a white line, in (e).

with no cavities. Most quartz layers are strongly sheared, which results macroscopically in the development of: (i) a foliation outlined by a white-grey colour striping and discrete thin (< 1 mm) biotite-decorated planes, subparallel (high strain: Fig. 5a) or oblique (low strain: Fig. 5b) to the layer boundary and (ii) a strong fibre-like lineation on the layer surface. Foliation in deformed quartz veins is usually planar, indicating a rather homogeneous strain distribution.

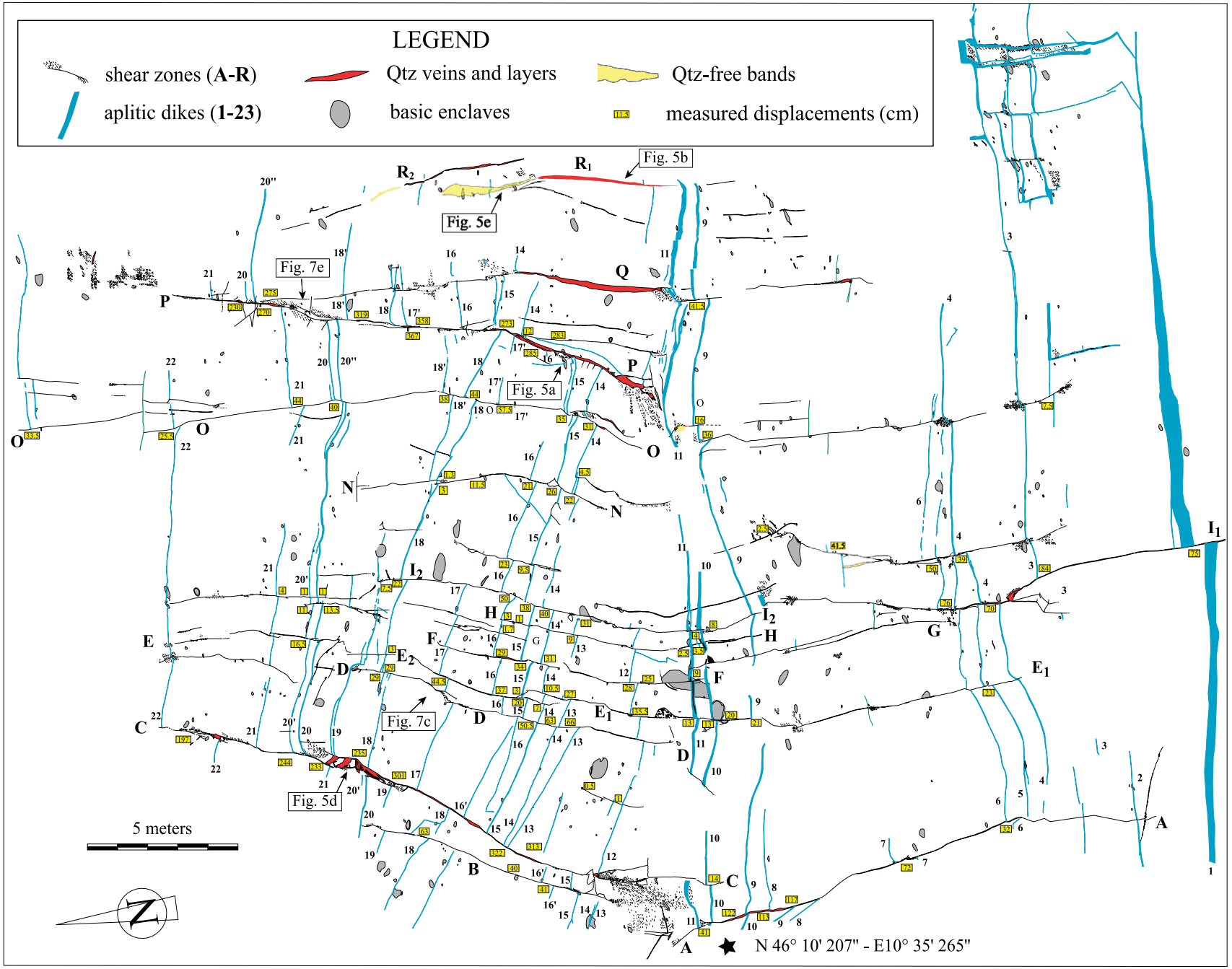

Fig. 3. Surface map of the studied outcrop in the Lobbia area. Shear zones are labelled with upper case bold letters (**A**–**R**) and aplite dykes with bold numbers (**1**–**23**).

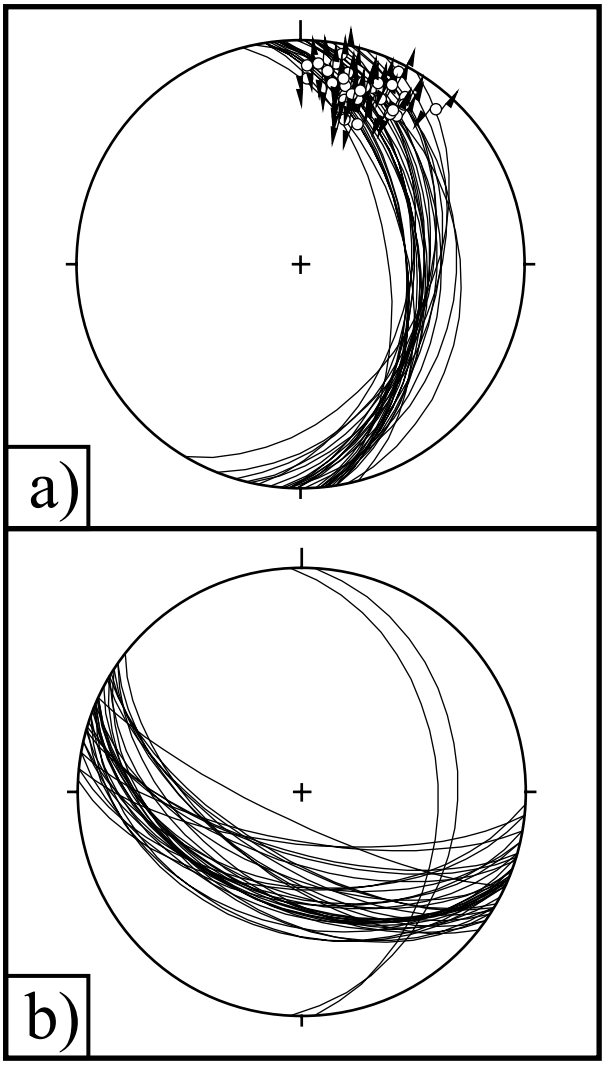

Fig. 4. Orientation (lower hemisphere, equal area stereonet) of ductile shear zones (a) and aplites (b) in the studied outcrop.

It is remarkable that: (i) the length of quartz layers or veins along shear zones in most cases greatly exceeds the maximum displacement accommodated by the shear zone itself (e.g. **L** is outlined by a 5-m-long continuous quartz vein of 1 cm mean thickness, but records a maximum displacement of 7.5 cm) and (ii) thick (and long) veins may be associated with very minor shear displacement (the thickest veins in the map are nearly undeformed). These observations indicate that quartz veins do not simply fill pull-apart domains developed at steps between adjacent parallel surfaces during their shear reactivation. In addition, it is worth noting that at the extensional step present between the overlapping en-échelon terminations of $\mathbf{E_1}$ and $\mathbf{E_2}$, quartz veins are not present along the splays (Fig. 5c). It follows that there is very little or no dilation at these sites despite the large displacement gradients measured along shear zones close to the extensional step (see below). In contrast, quartz layers are present along the $\mathbf{E_1}$ and $\mathbf{E_2}$ shear segments. This suggests that emplacement of quartz veins preceded ductile shearing. However, there are some exceptions. Quartz along **C** fills thick pull-apart veins forming bridges between adjacent subparallel slip surfaces and oriented approximately 45° to these planes within the extensional quadrant for sinistral shear along **C** (Fig. 5d). Similar cases of synkinematic opening of a quartz vein are rarely documented outside the map.

Discontinuous (en-échelon) thin (<1 cm thickness) quartz–chlorite veins are in rare cases present at the tips of shear zones (**I** and $\mathbf{H_3}$). They also have an orientation close to 45° to the shear plane and again lie in the extensional quadrant for a sinistral shear sense.

A local feature associated with quartz veins and fault-like shear zones is the presence of bands and domains of a darker colour than the normal tonalites (Fig. 5e), which are completely depleted in quartz. Bands have straight to irregular boundaries and their thickness is up to few decimetres. They extend subparallel to quartz veins from their tips ($\mathbf{R_1}$) or occur with a Riedel orientation beside the shear zones (e.g. aside $\mathbf{M_1}$), often surrounding or flanking a fracture. Quartz-free domains also form rather irregular zones (e.g. the rightmost part of **C** visible in Fig. 3) associated with the en-échelon steps between shear zones.

Pegmatite dykes consisting of quartz, feldspar, ±biotite, ±muscovite occur with the same orientation as shear zones_1 in the Lobbia area (Fig. 5f). They are usually deformed, developing S–C′ foliations and tend to strongly localize shear deformation, with only minor deformation of the adjacent tonalite, similar to the case for quartz layers as described above. In the studied outcrop, aplitic dykes with a N–S orientation are locally present (upper right part of Fig. 3) and tend to develop paired shear zones at their margins (cf. Mancktelow and Pennacchioni, 2005).

The numerous markers crosscut by the shear zones allows the displacement (d) to be estimated at different positions (ℓ) along the length of each shear zone. Marker separation, measured on the outcrop surface, may be assumed to closely approximate the real displacement as the stretching lineation of the shear zones is at a very low angle to the outcrop surface. This also allows enclaves to be used to estimate displacements. The displacement distribution along the different shear zones is reported in Fig. 6. The displacements mainly refer to offsets accumulated by the shear along fault-like segments. However, it may also include, as in the case of **P**, a minor component of heterogeneous shear outlined by the dragging of markers in the host tonalite immediately adjacent to fault-like planes. Implicit in the fact that several shear zones terminate within the map area, displacements vary along the shear zone length. There are two major shear zones in the map area, **A**–**C** and **P**, which display a maximum displacement of more than 3 m. The rest of shear zones have maximum displacements in the range of a few decimetres. Displacement distribution is either approximately symmetric about a central maximum (**F** and $\mathbf{I_1}$) or, more commonly, asymmetric (**A**, **B**, **D**, **N** and **P**) with a maximum shifted towards

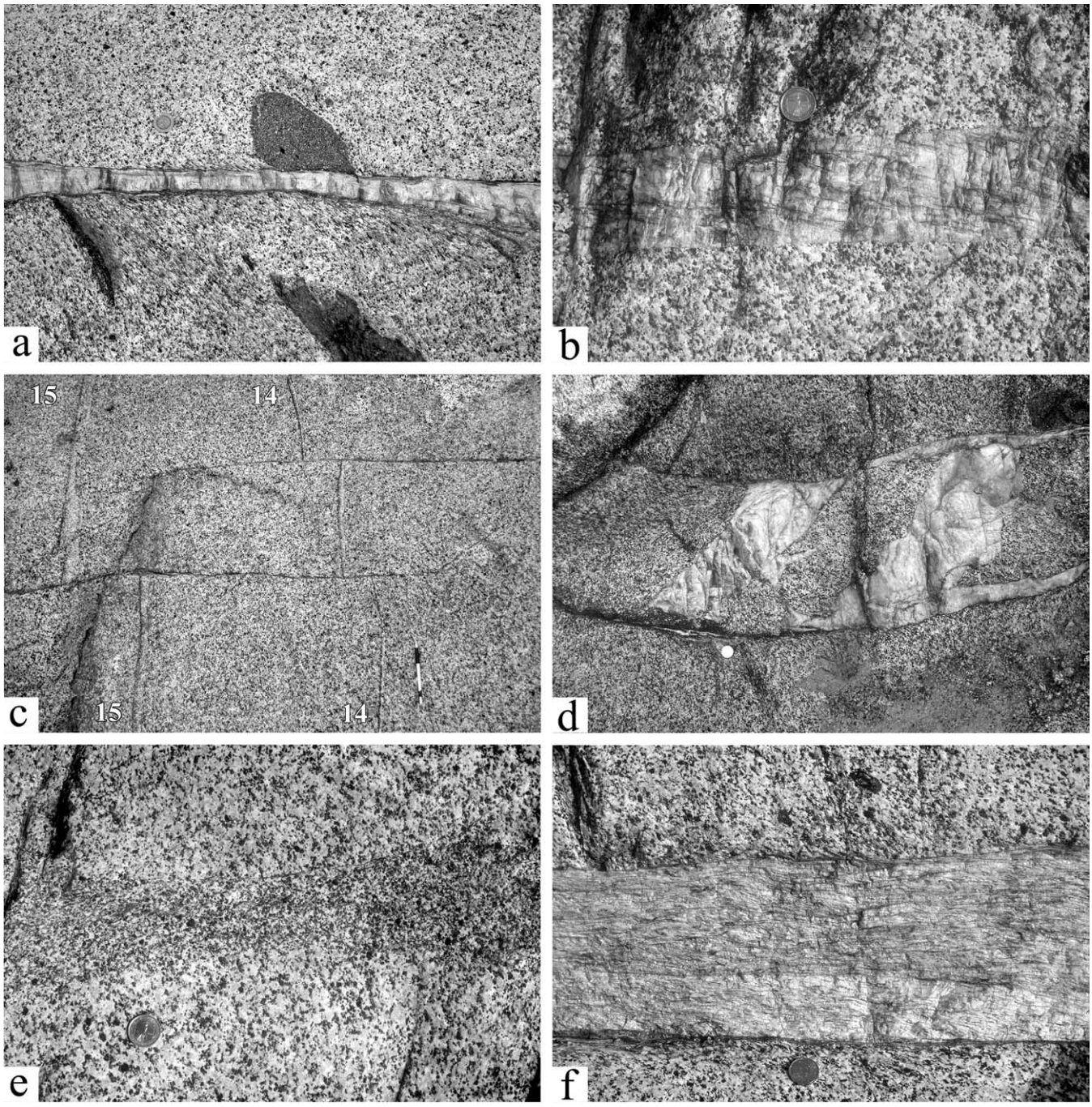

Fig. 5. Quartz veins, quartz-free bands and pegmatite dykes. (a) Quartz layer along **P**; the measured displacement of aplite **15–14** at this position of the shear zone is 2.73 m. (b) Oblique foliation in a slightly deformed quartz layer along $\mathbf{R_1}$; the measured displacement along $\mathbf{R_1}$ just 55 cm to the right of the photo is 30 cm. (c) Extensional step between adjacent tips of fault-like shear zones (**E**): note the linking oblique shear structures with no quartz filling. (d) Quartz veins bridging between adjacent subparallel confining shear planes along **C**. The veins are oriented at 45°, i.e. in an ideal orientation for sinistral simple shear along the shear planes. Note that quartz veins are also present along the shear planes. (e) Quartz-free band extending to the left of the thick quartz veins along $\mathbf{R_1}$. (f) Sheared quartz–feldspar pegmatite in tonalites outside the studied outcrop (GPS coordinates: 46°10′13.3″–10°34′48.5″). Sense of shear is sinistral in all photos. Scale: pencil (14.5 cm long) in (c) and coin (2.3 cm in diameter) in all the other photos.

one tip. In some cases, shear zones apparently accommodate nearly constant displacement along most of their length (**F**, $\mathbf{I_1}$ and **O**), but the displacement then rapidly decreases toward the shear zone tips (**F**, $\mathbf{I_1}$ and $\mathbf{I_2}$). In other cases, displacement increases continuously from the tips towards a single maximum (e.g. **A**). However, in general, the highest displacement gradients are found close to the shear zone tips. The displacement gradients ($\Delta d/\Delta \ell$) measured along many shear zones can be very high: values of 0.1–0.3 are rather common close to shear zone tips and displacement

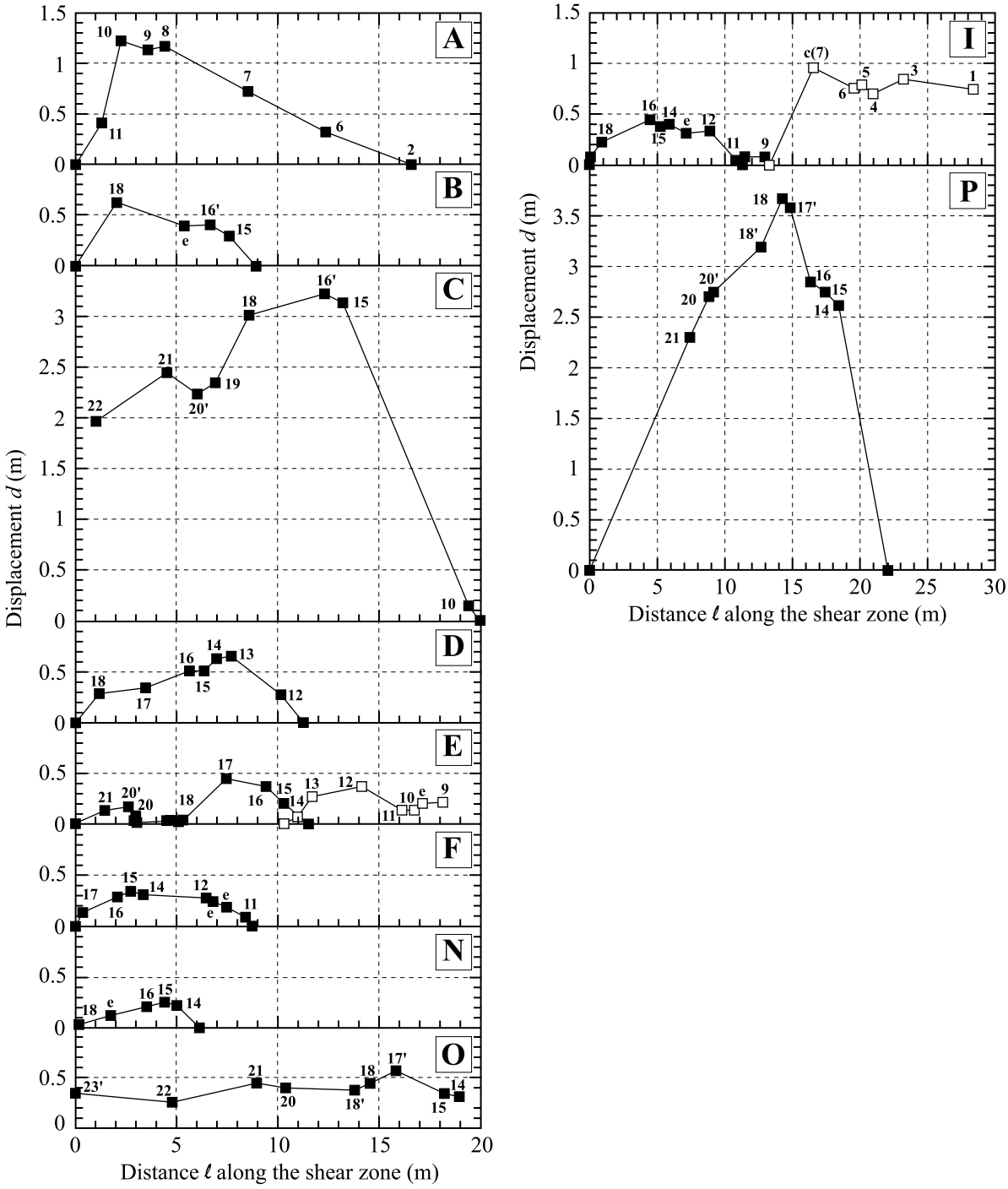

Fig. 6. Displacement distribution along different shear zones of the studied outcrop. See main text for a detailed explanation. The shear zones are identified by the uppercase bold letters in the upper right box of each diagram. For **E** (and **I**) the open and filled symbols refer to $\mathbf{E_1}$ ($\mathbf{I_1}$) and $\mathbf{E_2}$ ($\mathbf{I_2}$) segments, respectively. The numbers close to the symbols indicate the dyke used for the displacement estimate; e = enclaves. Note that the *x*-axis scale is different for the two plots on the right (shear zones **I** and **P**).

gradients as high as 0.5–0.8 are locally measured. Along most of the length of fault-like shear zones, the displacement variation is not accompanied macroscopically by any remarkable variation in shear zone thickness, distortion of the shear zone plane or, away from tips, by the development of a foliation in the adjacent tonalite.

Between the shear zones, tonalites are undeformed or display a weak foliation outlined by the shape preferred orientation of mineral aggregates and by the preferred elongation of enclaves. Foliation makes an angle of approximately 45° or greater (Fig. 2d) to shear zone boundaries, the orientation being consistent with the

sinistral sense of shear. As explained below, a foliation is typically developed at contractional bridges between adjacent en-échelon shear zone terminations, but domains of weakly foliated tonalites are also developed in the host rock between shear zones without a clear relationship to a particular location in the shear zone network.

At the map scale (and in general at the scale of several metres to a few tens of meters in the whole Lobbia area), fault-like shear zone segments are slightly non-coplanar, forming en-échelon arrays with non-overlapping or overlapping (much more common) terminations. This is a common characteristic of joints in many outcrops of the Adamello. Apparently, most en-échelon shear zones form right steps, i.e. contractional (using the terminology of Bürgmann and Pollard (1994)) for sinistral sense of shear and examples of extensional left-steps are uncommon. A composite contractional/extensional geometry is rarely found (e.g. left tip of **I**, but in this case the thin extensional splay is filled with quartz–chlorite and is probably later than the main shear deformation and foliation development on the contractional side). Contractional steps are characterized by the development of a foliation bridging between the adjacent shear zone terminations. Foliation usually abuts sharply against the bounding fault-like surfaces in contact with undeformed tonalite outside the jog. The geometry of contractional steps forms several different types. Fault-like shear zone terminations may stay straight at the contractional step (Fig. 7a) or display an outwards deflection of one (Fig. 7b: along **E** close to the intersection with **12**) or both terminations (Fig. 7c and d). In the most simple case, the dominant foliation is rather planar and is oriented at $\sim 45°$ to the fault-like surface within the jog, but a common feature is that the foliation becomes progressively steeper (up to 80°) away from the bridge as its intensity and the volume of affected tonalite decreases (Fig. 7a and b). Foliation may either be spread over the total length of the jog, forming lozenge-shaped domains (Fig. 7a) or, more rarely, may be relatively localized within a small thickness (normal to the foliation plane) of the foliated domain compared with the foliation length (Fig. 7c). The examples reported in Fig. 7a and b are common structures at bridges of minor fault-like shear zones accommodating displacements on the order of a few decimetres and are interpreted as relatively low strain contractional bridges (as roughly estimated by marker displacement or by the foliation intensity). Other contractional bridges have more complex foliation patterns. In some cases, they display strain localization towards the fault-like bounding shear plane. Localization is incipient in the bridge of Fig. 7a and well developed in the upper boundary of the large jog (approximately 4 m^2 in area) between **A** and **B**–**C**, as well as at the left termination of **P**. Intensely foliated zones are observed extending between separated (i.e. non-overlapping) en-échelon terminations of fault-like shears. In these cases, the foliation has a sigmoidal shape with an orientation, in the axial part of the shear zone, inclined at a low angle with respect to the trace of fault-like shear zone away from the bridge (Fig. 7d). It either still abuts rather sharply against the bounding fault-like planes or extends 'outside' the jog as a weak foliation.

A particular feature of **P** is that it displays a bend associated with a complexly foliated domain that corresponds with the displacement of aplites **20**–**20**″ (Fig. 7e). Along this segment, displacements are remarkably high (2.70–2.75 m) and do not correspond to any major minimum in the displacement distribution curve (Fig. 6), being intermediate between the displacements along the fault-like extension immediately to its left and right sides. In detail, the sigmoidal continuous foliation is asymmetrically developed around an ultramylonitic dark layer that connects the fault-like shear zones. On the right (southern) part of the shear zone step, the ultramylonic dark layer wraps around a domain similar to quartz-free bands within the tonalites. Overall, these features suggest that foliated portions with a well-developed sigmoidal foliation represent high strain examples of an evolving contractional step between en-échelon stepped terminations of fault-like shears.

4. Microstructure

4.1. Tonalites

4.1.1. Undeformed tonalites and quartz-free bands

The Avio tonalites mainly consist of Pl_1[1] (45–50% volume), Qtz_1 (25–30%), Bt_1 (15–20%) and Kfs_1 (1–5%). *Pl* occurs as euhedral zoned crystals with relict anorthite-rich corroded cores (80–95 to 65% anorthite from inner to outer core) surrounded by oscillatory-zoned mantles with a composition in the range of 58–30% anorthite. *Kfs* forms monocrystalline interstitial zones. Details on the petrography of the tonalites can be found in Bianchi et al. (1970).

The mineral composition and microstructure of quartz-free bands or domains is apparently identical to that of normal tonalites except for the total absence of quartz. The texture is magmatic without any sign of solid-state dissolution features.

4.1.2. Foliated tonalites

Bt_1 has a lensoidal to irregular shape elongated parallel to foliation The lensoidal shape develops when the biotite cleavage is subparallel to foliation, whereas the irregular shape results from deep embayments, due to indentation of *Pl*, locally associated with the development of fine-grained symplectitic intergrowths of Pl_2 and *Tit* at the Pl_1–Bt_1 boundary. Bt_1 displays undulose extinction and incipient recrystallization that, in lens-shaped Bt_1, is especially developed at the tapering tips.

[1] Mineral abbreviations are: *Bt*=biotite; *Ilm*=ilmenite; *Kfs*=K-feldspar; *Pl*=plagioclase; *Qtz*=quartz; *Tit*=titanite. The subscripts 1 and 2 refer to successive generations and, in particular, to magmatic (1) and syn-deformation (2) mineral phases, respectively.

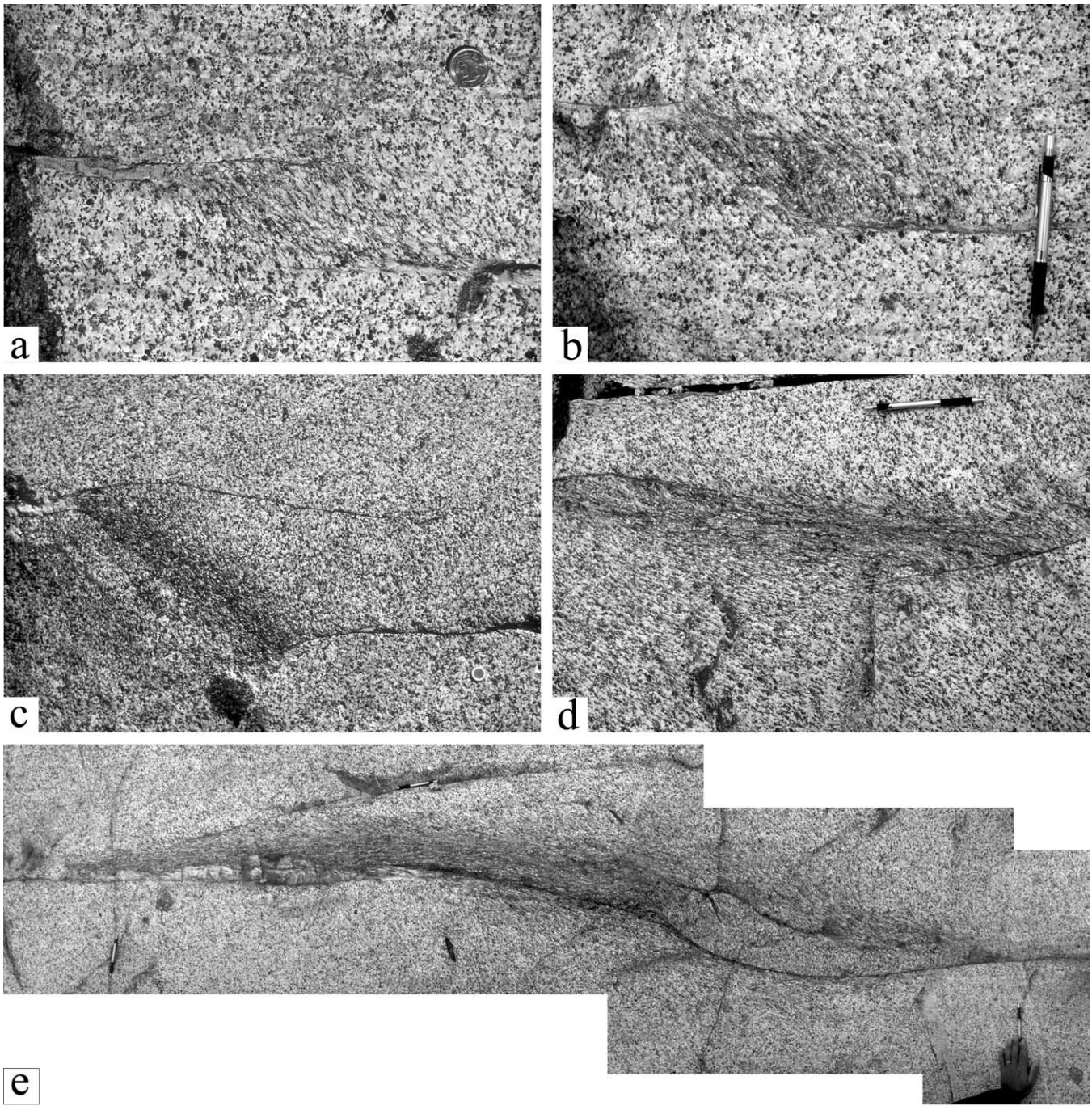

Fig. 7. Contractional bridges at en-échelon shear zone terminations. (a) Contractional bridge with no deflections of shear zone tip; foliation in the bridge is typically at around 45° to the shear zone plane. Note totally undeformed tonalite outside the jog (above and below the bounding fault-like shear zone termination. (b) Contractional bridge with deflection of the upper shear zone termination. The contractional bridge is located along $\mathbf{E_1}$ at the intersection with **12**. (c) Localized foliation at the contractional step along the shear zone **D** associated with a deflection of the fault-like bounding shear planes. (d) Strongly foliated domains with a tendency to develop sigmoidal foliation between separating tips of stepped fault-like shear zone terminations. (e) Detail of the foliated step along the shear zone **P**; the foliated step connects with fault-like shear zone segments on both sides and develops a sigmoidal-shaped foliation surrounding a dark thin ultramylonitic horizon continuous along the bridge (on the right, a pair of ultramylonitic horizons wrap around an elongate domain of quartz-free tonalites). Sense of shear is sinistral in all photos. Scale: coin (2.3 cm in diameter) in (a) and (c), and pencil (14.5 cm long) in (b), (d) and (e).

Quartz exhibits a range of microstructures: typically it is coarse-grained, displays high-T serrated grain boundaries with stepped facets (forming angles close to 90°) and does not present any optical sign of internal plastic deformation. As in quartz veins (see later), adjacent quartz grains could be strongly 3D interpenetrated but 2D sections are preferentially elongated parallel to foliation. Other quartz grains have more

serrated grain boundaries and display some internal coarse polygonization and incipient grain size reduction due to dynamic recrystallization.

Plagioclase is undeformed except for the local presence of a few dilatant cracks, preferentially oriented at a high angle to foliation and filled with quartz–feldspar, which conceivably developed during movement of late magma during deformation (e.g. Bouchez et al., 1992; Vernon et al., 2004). K-feldspar displays local overgrowth by small myrmekite lobes.

4.1.3. S–C′ mylonites and mylonites

Observations were made on thin sections parallel to stretching lineation (*X*-axis) and orthogonal to mylonitic foliation (*X*–*Y* plane). Along strain gradients, tonalites display a transition, with increasing deformation, from composite S–C′ fabric to a prominent mylonitic foliation parallel to the shear zone boundary. The transition is usually rather sharp.

4.1.3.1. S–C′ mylonites. In S–C′ mylonites, S planes are outlined by compositionally different domains consisting of: (i) Qtz_2, (ii) $Bt_2 \pm Ilm \pm Pl_2$ and (iii) $Pl_2 + Qtz_2 \pm Kfs$ The latter develop as pressure shadows or tails attached to Pl_1 porphyroclasts (mm's in size) wrapped around by (i) and (ii).

Qtz_1 is deformed into elongated ribbon domains of dynamically recrystallized aggregates of Qtz_2. The grain size and shape of Qtz_2 is quite variable as a result of the highly heterogeneous strain patterns induced by the presence of *Pl* porphyroclasts wrapped around by foliation. Qtz_2 is equant to (more commonly) elongate, defining a strong shape preferred orientation (SPO) inclined at a relatively high angle ($>45°$) to the compositional layering. In SEM secondary electron images of broken surfaces (see Mancktelow and Pennacchioni (2004) for details on the technique), Qtz_2 microstructure is often bimodal with elongate grains (a few 100's μm long) surrounded by a mantle of small (a few μm's in diameter) polygonal grains. Qtz_2 have a strong CPO with a *Y*-maximum of quartz c-axes, as inferred by the close-to-extinction orientation of most grains under crossed polars.

Bt_1 occurs as common mica fish and is recrystallized into aggregates of oriented $Bt_2 \pm Ilm$ outlining the foliation. It shows rim replacement by symplectites of Pl_2–*Ilm*–Bt_2 when in contact with Pl_1 (Fig. 8b). Bt_2 also form in pressure shadows around *Pl* porphyroclasts.

Pl_1 occurs as well-rounded unaltered porphyroclasts with no (or very weak) internal plastic deformation up to high strain. When inside Bt_2-rich layers, *Pl* shows interpenetration in pressure shadows with *Bt*. When included in *Qtz* domains, *Pl* shows fracturing (initial deformation) along extensional cracks. These openings, as well as pressure shadows, are commonly filled by *Kfs*.

Kfs is preserved in pressure shadows around Pl_1 porphyroclasts, or within thick tails connecting pulled apart *Pl*, or associated with mosaic or vermicular myrmekitic $Pl_2 + Qtz_2$. In pressure shadows the *Kfs*–Pl_1 boundary is often free of myrmekites, which are instead present at the contact of *Kfs* with the *Qtz* folia wrapping around *Pl*. Myrmekites also form as isolated irregular regions in *Kfs*. With increasing strain and porphyroclast separation, pressure shadows are stretched to thin δ-shaped tails mainly composed of a fine polygonal $Pl_2 + Qtz_2$ aggregate. *Kfs* is still preserved as small triangular pressure shadows against Pl_1 or, within the tails, as irregular relicts and polygonal grains.

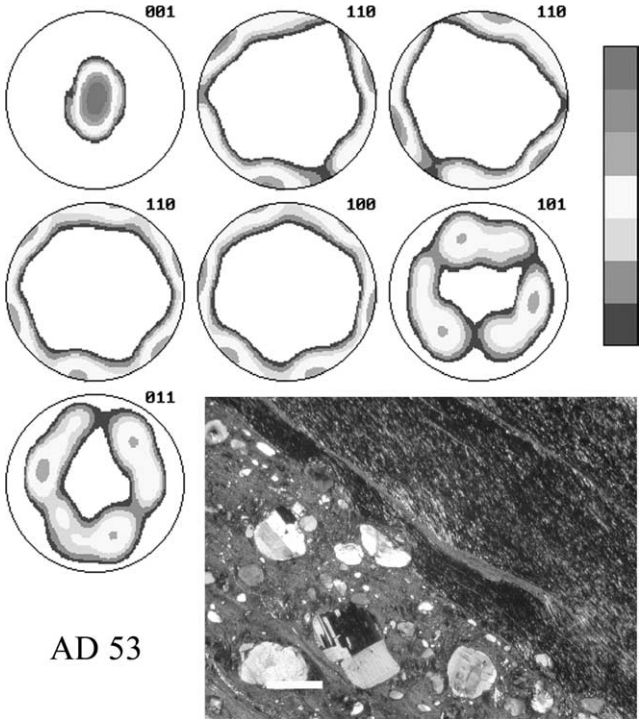

Fig. 8. Crystallographic preferred orientation (CPO) of quartz mylonite AD53 determined by X-ray texture goniometry. The projection is into the upper hemisphere and the foliation is oriented EW and vertical, with the lineation horizontal. Contours are logarithmic, ranging from 0.01 to 5 times a uniform distribution. The photo displays the optical microstructure under crossed polars of the analysed sample (view is a *XZ* section; sense of shear is sinistral; scale bar is 1 mm; foliation is oriented NE–SW). The quartz mylonite (upper right part) consists of an aggregate of Qtz_2 (recrystallization is complete) with a strong oblique shape fabric and a dominant dark interference colour consistent with the sharp c-axis *Y*-maximum of the CPO. The tonalite mylonite (lower left corner) contains millimetre-sized rounded porphyroclasts of Pl_1 set in a fine-grained matrix of $Bt_2 + Qtz_2 + Pl_2 + Ilm$.

4.1.3.2. Tonalite mylonites. Mylonites consist of a relatively homogeneous matrix (grain size <10 μm) of $Bt_2 + Pl_2 + Qtz_2 \pm Ilm$ still including abundant well-rounded unaltered *Pl* porphyroclasts ranging in size from a few mm's to 10's–100's μm. Rootless folds of thin discontinuous Qtz_2 layers are also present in the matrix.

4.2. Quartz veins

In the least deformed veins, quartz is coarse-grained (several cm's) and displays stepped or serrated grain boundaries. Quartz grains are strongly interpenetrated in 3D and, in thin sections, a single grain may appear as several different isolated island grains of identical crystallographic orientation within (and including islands of) neighbour grains (Urai et al., 1986). The shape profile of island grains is complexly interlocked, locally resulting in 'dendritic' geometries dominated by stepped grain facets generally forming angles close to 90°. Some grains display coarse polygonization and deformation lamellae. Incremental deformation produces fine-grained aggregates starting from grain boundaries.

Quartz mylonites derived from veins range in texture from homogeneous, consisting of a rather unimodal fine-grained (grain size in the range of few 10's of μm) aggregate of Qtz_2, to domainal mylonites consisting of an alternation of recrystallized Qtz_2 aggregates and monocrystalline ribbons parallel to the mylonite boundary. In this latter case, Qtz_2 aggregates display an extinction banding mimetic on the former ribbon structure. Qtz_2 aggregates have an oblique shape fabric and a strong crystallographic preferred orientation.

4.2.1. CPO in quartz mylonites

The CPO of dynamically recrystallized Qtz_2 in a quartz mylonite was determined by X-ray texture goniometry. The analysed sample (AD53_99) is a pure quartz layer outlining the median zone of a shear zone and consists of a completely recrystallized aggregate of fine-grained Qtz_2. Texture data are reported in Fig. 8. The X-ray pole figure obtained for the sample is nearly a 'single-crystal' type with a strong single *Y*-maximum of c-axis consistent with prism ⟨a⟩ slip system (Schmid and Casey, 1986; Mancktelow, 1987).

4.3. Pegmatites

Deformed pegmatites display S–C′ composite foliations outlined by layers of ultra-fine-grained aggregates of $Pl_2 + Qtz_2$ (recrystallized myrmekites), of recrystallized quartz and biotite-rich or (less commonly) white mica-rich aggregates. Foliation planes wrap around abundant *Kfs* porphyroclasts, which are rimmed by pervasive lobes of vermicular myrmekite along the boundaries facing S planes. Sigmoidal mica fish of biotite and white mica are locally preserved along S planes adjacent to shielding *Kfs* porphyroclasts.

5. XRF compositions

Whole-rock geochemical analyses of major and trace elements of undeformed tonalites (5 samples), quartz-free bands (2 samples), foliated tonalites (6 samples), S–C′ mylonites (2 samples) and mylonites (4 samples) were performed by X-ray fluorescence (XRF) spectroscopy with a Philips PW2400 equipped with Rh tube (Department of Mineralogy and Petrology, University of Padova). LOI were determined from weight lost after ignition at 860 °C for 20 min and at 980 °C for 2 h. FeO was determined by permanganometry.

The major element average compositions of the different sample categories are shown in Table 1 (the original major and trace element data can be found in the online version of this paper doi: 10.1016/j.jsg.2004.11.008) and plotted in the isocon diagram of Fig. 9 to reveal possible compositional variations during deformation (Grant, 1986). The comparison between the average compositions of samples from differently strained regions (except for quartz-free bands) and the low values of standard deviation indicate: (i) a very homogeneous composition of the tonalite protolith and (ii) that no geochemical changes occurred during deformation. Quartz-free bands have a lower amount of SiO_2 and higher amounts of all other major elements than undeformed/deformed tonalites. However, the same composition of tonalites may be obtained from that of quartz-free bands by simple addition of SiO_2: the last column in Table 1 is calculated from the composition of quartz-free bands by just increasing SiO_2 to 95 and re-normalising oxide concentrations to 100%. In the isocon diagram (Fig. 9), the element concentrations of the differently deformed rocks and of corrected (SiO_2-added) quartz-free bands plotted against concentration of the same oxides in the undeformed tonalites lie nearly perfectly along the same straight line with a slope of 1 passing through the origin (i.e. no mass

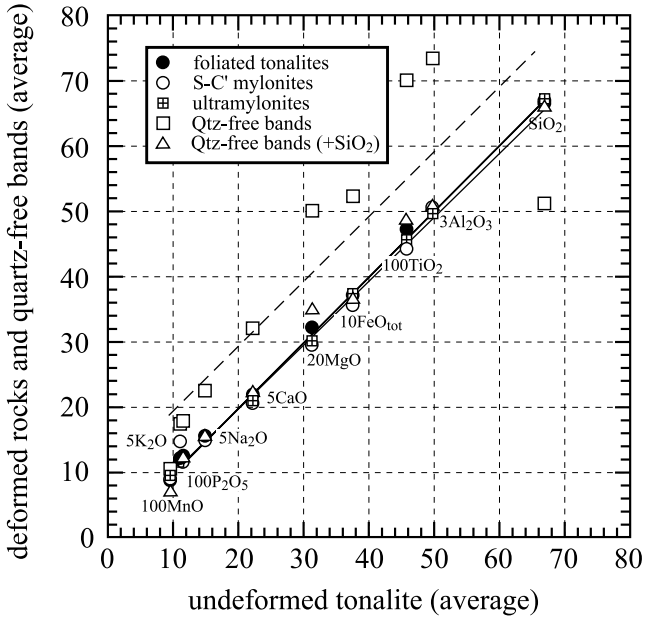

Fig. 9. Isocon plot comparing the average major elements composition of differently deformed tonalites and quartz-free bands with that of undeformed tonalites. The *m*, *q* and R^2 values of the best-fit lines of data points (which overlap in the plot, except for the dashed line relative to quartz-free bands) are reported in Table 1.

Table 1
Average major element (wt%) XRF analyses of the differently strained tonalites (undeformed to ultramylonites) and quartz-free bands. The s.d. acronym stands for standard deviation. The last column in the table is the composition of quartz-free bands with SiO_2 increased to 90% from the original amount (all oxides re-normalized to 100%). The *m*, *q* and R^2 values (bottom rows) are the parameters (slope, *y*-intercept and goodness-of-fit value) for the best-fit linear regression lines of data in the isocon plot of Fig. 8

Strain	Undeformed tonalite		Foliated tonalite		S–C′ mylonite		Ultra-mylonite		Qtz-free bands		Qtz-added
Number of samples	5		7		2		4		2		
		s.d.		s.d.		s.d.		s.d.		s.d.	
SiO_2	66.85	*0.96*	66.43	*1.13*	66.71	*0.30*	67.18	*0.81*	51.16	*0.14*	66.05
TiO_2	0.46	*0.05*	0.47	*0.04*	0.44	*0.00*	0.45	*0.02*	0.70	*0.03*	0.49
Al_2O_3	16.61	*0.36*	16.92	*0.59*	16.88	*0.25*	16.52	*0.36*	24.44	*0.28*	16.99
FeO	3.43	*0.29*	3.41	*0.30*	3.41	*0.03*	3.37	*0.23*	4.59	*0.11*	3.19
Fe_2O_3	0.33	*0.08*	0.31	*0.22*	0.15	*0.04*	0.35	*0.11*	0.63	*0.06*	0.44
MnO	0.10	*0.01*	0.09	*0.01*	0.09	*0.00*	0.09	*0.01*	0.10	*0.01*	0.07
MgO	1.57	*0.18*	1.61	*0.15*	1.48	*0.03*	1.51	*0.10*	2.51	*0.09*	1.74
CaO	4.46	*0.15*	4.41	*0.16*	4.12	*0.10*	4.19	*0.11*	6.41	*0.08*	4.46
Na_2O	2.96	*0.05*	3.09	*0.15*	2.99	*0.10*	3.06	*0.14*	4.48	*0.09*	3.11
K_2O	2.21	*0.11*	2.42	*0.11*	2.94	*0.09*	2.34	*0.14*	3.48	*0.02*	2.42
P_2O_5	0.12	*0.01*	0.12	*0.01*	0.12	*0.01*	0.12	*0.01*	0.18	*0.01*	0.12
LOI	0.91	*0.07*	0.74	*0.17*	0.67	*0.02*	0.81	*0.21*	1.32	*0.02*	0.92
Total	100.00		100.00		100.00		100.00		100.00		100.00
m			0.994		0.999		1.005				0.988
q			0.048		0.010		−0.043				0.097
R^2			1.000		1.000		1.000				1.000

transfer) (see *m*, *q* and R^2 values for the best fit linear envelopes in Table 1).

6. Discussion

6.1. P–T conditions of ductile deformation

Several factors point to relatively high *T* metamorphic conditions (amphibolite facies) during the dominant ductile deformation of the Lobbia tonalites. These include:

1. Absence of plagioclase alteration and stability of relatively anorthite-rich Pl_2 ($An_{38–40}$: determined by EDAX analysis with a CamScan Mx 2500). Such high-Ca plagioclase occurs as a mineral component in the ultramylonite matrix and, associated with quartz, in the strain-induced myrmekites and myrmekite-derived poly-mineralic fine-grained recrystallized aggregates. Temperatures for myrmekite formation are not well constrained, but are usually considered typical of upper greenschist to amphibolite facies conditions. Myrmekites has been inferred to have grown at 450–500 °C (Tribe and D'Lemos, 1996) and 500–670 °C (Wirth and Voll, 1987), based on temperatures indicated by other minerals in the same rocks as myrmekites.
2. The CPO of synkinematically recrystallized quartz aggregates in tonalite mylonites and associated quartz mylonites show a single *Y*-maximum of c-axes, indicative of prism ⟨a⟩ slip. This texture is typical of amphibolite facies metamorphic conditions ($T > 500$ °C: e.g. Stipp et al., 2002; Mancktelow and Pennacchioni, 2004).

Pressures of 0.25–0.3 GPa (corresponding to a depth of 9–11 km for a rock density of 2650 kg m^{-3}) were estimated for contact metamorphism along the northern border of the Presanella, based on the absence of melting during reactions producing K-feldspar + sillimanite and on the observed polymorphic phase transformation of andalusite to sillimanite (Werling, 1992). These pressure conditions (or slightly lower) may be assumed also for ductile deformation in the Avio tonalites.

6.2. Nucleation of shear zones

The overall mesoscopic observations indicate that the Lobbia shear zones nucleated on a former set of subparallel joints. Joints with the same orientation as the shear zones are pervasive throughout the whole Avio intrusion. Joints are arranged en-échelon at the outcrop scale (several meters to tens of meters) and have a spacing on the order of decimetres to a few meters, characteristics which are inherited by the shear zones. Joints are initially reused as fault-like shear zones with very minor plastic deformation of the wall rock along most of the shear zone length. In most cases, the en-échelon joint terminations are slightly overlapping and there is no indication for further propagation of fracture tips during subsequent ductile shearing.

Some joints were intruded, before the ductile

reactivation, by pegmatite dykes or filled with quartz veins with dimensions up to several meters in length (tens of meters in the case of pegmatites) and a few decimetres in thickness. However, it must be emphasized that joints without any quartz filling are present in the studied outcrop and are also ductilely reactivated. Ductilely reactivated joints (fault-like shear zones) are also common in other areas of the Avio intrusion and in all the Adamello intrusive bodies, where quartz veins are usually rare or absent.

Both pegmatites and quartz veins were weaker than tonalites, under the synkinematic conditions of ductile deformation, as they tend to localize strain with only minor involvement of tonalite at the layer boundary, at least during initial stages of shearing. The weakness of pegmatites compared with the finer grained tonalites is due to the efficiency of grain size reduction by development and recrystallization of myrmekites, which is pervasive in pegmatites, inducing a strong strain softening (Tsurumi et al., 2003).

6.3. Time relationships between quartz veining and ductile shearing

Emplacement of quartz veins was mainly before ductile shearing as suggested by field observations and by geochemistry: (i) when a marker displacement is observed across a quartz vein, the vein is always deformed; (ii) quartz does not normally fill splay veins or pull apart structures kinematically related to sinistral shear, but rather occurs along joint planes developing as dilational veins; (iii) no chemical change occurs during foliation development in tonalites, apparently excluding element mobility and therefore a synkinematic in situ production of SiO_2 by dissolution in high strain domains. Quartz-free bands are a very likely source of vein quartz. The quartz-free bands have a mineral composition that is identical to that of tonalites except for the absence of quartz and whose oxide ratios (excluding SiO_2) are identical to those of normal tonalites. As noted above, the tonalite composition can be obtained from that of quartz-free bands by simple addition of SiO_2. Whatever the mechanism of silica extraction, the texture of quartz-free bands is igneous and points to a syn- or late-magmatic phase of quartz leaching/precipitation, therefore preceding solid-state deformation along shear zones.

There are some exceptions to the general geometry of quartz veins described above, especially in the case of (ii), as can be seen for example in Fig. 5d. This and a few other examples suggest a constant stress field during quartz vein emplacement and ductile shear reactivation of joints. The observations suggest that: (i) quartz vein emplacement slightly predated (and partly overlapped) ductile shearing and (ii) shear along the joints was not simultaneous. A diachronous reactivation of joints may perhaps explain some structural features such as the patchy distribution of weakly foliated tonalites between fault-like shear zones apparently unrelated to contractional bridges (see discussion at the end paragraph of Section 6.4).

The quartz–chlorite veins, locally present in the extensional quadrants of shear zone tips, can be referred to a later, lower T, weak reactivation of the mylonites, under the same stress field. In fact, chlorite is more consistent with the fracture-related alteration typically associated with cataclasites, which overprint ductile shear zones along the adjacent fault zone (Di Toro and Pennacchioni, in press).

6.4. Distribution of ductile strain resulting from nucleation on precursor joints

The presence of pre-existing planes of weakness produces a strong localization and partitioning of the bulk deformation. From the total displacement of the aplite dyke **14** across the whole thickness of the mapped outcrop, a bulk shear strain of $\sim$0.5 may be calculated. This estimate is a minimum value for bulk shear strain as it only takes the cumulative dyke displacements due to fault-like shear zones into account. However, given the development of only a weak foliation in the intervening tonalite blocks between fault-like planes and the subparallel arrangement of dyke segments, any additional rotational component of homogeneous strain must be very low and the bulk strain close to the estimated value of $\sim$0.5. If the same amount of bulk shear strain is assumed for the entire outcrop area, it means that along the right (southern) border of the outcrop, where dyke **1** displays a unique displacement of 75 cm along $\mathbf{I_1}$, the total strain has to be accommodated by distributed development of a very weak fabric corresponding to the bulk γ of $\sim$0.5. In contrast, along fault-like shear zones, shear strains as high as several 100's are estimated. This means that differences of about three orders of magnitude in strain rates may have occurred at different locations in the outcrop, assuming constant bulk strain rate boundary conditions. Given the stress/strain rate sensitivity of recrystallization mechanisms during crystalline plasticity (e.g. see transition in quartz recrystallization regimes determined experimentally under constant T but variable strain rates by Stipp and Tullis (2003)), this could possibly be recorded in contrasting microstructures in low and high strain domains. For example, quartz microstructures in foliated tonalites, indicative of grain boundary migration recrystallization, may reflect low strain rates compared with microstructures in quartz mylonites, which are more typical of subgrain rotation recrystallization. The use of quartz microstructures as geothermometers in rocks showing highly heterogeneous strain distribution must be used with caution. A different explanation for the different quartz fabric between foliated tonalites and mylonites is that they developed under different T conditions during cooling of the pluton (see below).

Joints are discrete structures with a length in the range of several meters to a few tens of meters and mostly form an en-échelon pattern, usually with minor overlaps between

joint terminations. In general, these terminations form right-handed steps, which are contractional for the overprinting sinistral shear. Sheared joints accommodate displacements on the order of a few decimetres to a few metres in the central portion, which decrease to zero at joint tips, usually developing very high displacement gradients towards shear zone terminations. The measured displacement gradients close to shear zone tips are commonly in the range 0.1–0.3 (but can be as high as 0.8), consistent with the high values (up to 0.40–0.48) reported by Christiansen and Pollard (1997) in two ductile shear zones within Sierrean granites (California), which are the only published data at present. The difference in displacement must somehow be accommodated by deformation of the host tonalites. Most differential displacement is clearly accommodated by development of a foliation at the contractional steps with little or no development of quartz veining to form splay structures in the opposite extensional quadrant at the shear zone tips. Concentrated deformation at joint terminations and contractional jogs reflects the perturbed stress field at these sites, as shown in numerical (Bürgmann and Pollard, 1994; Nemčok et al., 2002) and analogue models (Connolly and Cosgrove, 1999a,b). Geochemical analyses of undeformed to mylonitic tonalites indicate that no mass transfer assisted deformation. Therefore, as material is displaced into the jog, geometric compatibility under isochoric (constant volume) plane strain conditions implies that material is displaced laterally, deflecting the shear zone tips (as observed in Fig. 7b and c and in several other cases). Alternatively, non-plane strain accommodation may occur, with material moving out of the *XZ* plane. This is consistent with the absence of distortion of the bounding fault-like planes, as in the case shown in Fig. 7a. These two end-member strain fields (Ramsay and Allison, 1979, fig. 14) combine in different ways to form the range of structural patterns observed at contractional sites in the Lobbia outcrops. The contrast in structural patterns developing from initially identical geometric configurations (same separation/overlap ratios at joint en-échelon terminations) within a rather homogeneous protolith suggests that even small initial heterogeneities may cause stress perturbations, which result in severe bifurcation in the strain paths during the following evolution. This has to be taken into account in any attempt at modelling these structures. The variable 2D patterns in the outcrop may also result from sectioning at different levels of a 3D structure.

The segmentation and right-stepped en-échelon geometry of joints hindered easy strain accumulation by ductile slip along the pre-existing discontinuities. Without any propagation of joint/shear zone tips, ductile reactivation under isochoric water-deficient conditions can only be achieved by development of a geometric connectivity of fault-like segments at the contractional side of joint terminations, which is also favoured by the preferential right-stepped en-échelon arrangement of precursor joints. The development of a foliation in the contractional bridges (determined by the stress concentration at these sites) is a necessary precursor to involvement of the contractional jogs in active shear deformation by inducing a strain softening of these domains. Strain softening may be due mainly to synkinematic grain size refinement processes such as (i) development and recrystallization of myrmekites and (ii) recrystallization of quartz and biotite. With increasing strain, the amount of shear accommodated along the foliated bridges increases as foliation is rotated from the initial 45° orientation to a lower angle with respect to the average shear plane, developing the typical sigmoidal shape of continuous shear zones. Because a component of shear is taken up by foliated contractional bridges, the displacement gradients along the shear network tend to decrease and fault-like shear zone tips are moved apart. In the case of an initial slight overlap of joints (which is rather common), shear along foliated contractional bridges results in a separation of the fault-like shear zone terminations (as seen in Fig. 7d), which then display a connection by a continuous shear zone. This explains the rather common field observation, in the Lobbia area, of transitions and alternation 'along strike' between extremely localized fault-like shear zones and continuous shear zones. Strongly foliated tonalites with an S to S–C′ fabric sharply confined between fault-like planes could develop in a similar way in the case of highly overlapping joints. With increasing strain, these domains may evolve into discontinuous mylonitic horizons with sharp contacts against undeformed tonalites.

Displacement gradients along fault-like shear zones also exist away from contractional bridges and must be accommodated by some deformation of the country rock. Joints were not necessarily reactivated at the same time and therefore stress interaction could occur between relatively distant joint segments rather than those that were closest together. The mechanical properties of different joints and of different segments of the same joint were probably not the same due to the presence or absence of quartz veins or pegmatite dykes. All these factors can be responsible for more complex stress perturbation fields and for 'strain bridging' between different elements of joint arrays beyond the overlapping en-échelon joint terminations. This may be the reason for the non-localized weak foliation present in the outcrop between the fault-like shear zone planes. Alternatively, weakly foliated domains in tonalites between the joints may have developed during higher *T* deformation than the dominant localized ductile shear reactivation of joints. Both the high *T* and/or low strain rate conditions of non-localized deformation are consistent with the grain boundary migration quartz microstructure of weakly foliated tonalites. In weakly foliated tonalites, the degree of deformation-induced grain size refinement is extremely poor and does not result in any localized deformation with increasing strain.

6.5. The brittle-to-ductile deformation of the Lobbia as a characteristic structural evolution during cooling: comparison with previous works

A series of papers (Segall and Pollard, 1983; Segall and Simpson, 1986; Martel et al., 1988; Bürgmann and Pollard, 1994; Christiansen and Pollard, 1997; Segall, 1998) have described shear zones within granitoids of the Sierra Nevada, California (and near Roses, Spain: Segall and Simpson (1986)), which nucleated on pre-existing joints or mineral-filled (epidote, chlorite, quartz and zeolites) dilatant fractures. Bürgmann and Pollard (1994) interpreted brittle fracturing (splay fractures) and ductile fabrics present at 'fault' terminations as coeval, developing at extensional and contractional quadrants of fault tips, respectively, due to a pressure-dependent constitutive behaviour under temperature conditions close to brittle–ductile transition. Also, they suggested a temperature-dependent change in the typology of shear zone terminations (see fig. 13 of Bürgmann and Pollard (1994)) from side-by-side occurrence of quartz-filled wing veins and foliated domains at conditions close to brittle–ductile conditions, to symmetric foliated domains prolonging the tips of fault-like shear segments at higher T (close to the contact with a younger plutonic body). Despite the striking similarities in many structural features between the Lobbia shear zones and those described in the papers cited above, there are also some significant differences. In the Lobbia outcrops: (i) shear zones do not overprint former epidote, chlorite and zeolite veins that, in contrast, developed later (and at lower T) than the major shearing event; (ii) quartz veins mainly predate ductile shearing and there is no formation of extensive splay fractures at joint tips or bridging between adjacent fault-like planes; (iii) synkinematic temperatures are well above the brittle–ductile transition conditions assumed for deformation in Roses/Sierrean granites; (iv) despite the relatively high temperature conditions, foliations at shear zone terminations are always developed asymmetrically with respect to the shear plane and in the contractional quadrant, rather than forming symmetric shear zones propagating from the shear zone tip.

The similarity of many structural features suggests that the Lobbia and Sierrean/Roses granitoids followed a similar brittle-to-ductile deformation evolution, which could represent a characteristic mode for the structural evolution of granitic intrusions during cooling. The very early (late-magmatic or early post-magmatic) development of pervasive joints in a cooling pluton and the rapid cooling due to the relatively shallow intrusion depth give rise to characteristic structural patterns during the ductile deformation, which can be considered as representative of this particular structural environment.

However, the differences in the structural features listed above need to be explained. At least part of the ductile deformation in the Sierra Nevada probably developed under relatively high T (upper greenschist to amphibolite facies) given the stability of biotite, the microstructure of quartz (see fig. 5 in Bürgmann and Pollard (1994)) and the probable synkinematic development and recrystallization of myrmekites. In the case of a simple cooling history, this is not consistent with nucleation on epidote-, chlorite- and zeolite-bearing fractures, which are stable under relatively low grade conditions, unless brittle features developed during a previous stage of pluton cooling and were later overprinted by shearing during re-heating related to emplacement of the adjacent intrusion. Re-heating by a later shallow intrusion is unlikely given (i) the low thermal conductivity of rocks and (ii) that no thermometamorphic effects are described in the undeformed granitoids hosting the shear zones. A possible interpretation is that deformation fabrics and metamorphic associations formed during decreasing temperatures are telescoped within the same mylonitic horizons, which are continuously reactivated during each deformation increment/event as preferential planes of weakness.

In the Lobbia area, the absence of splay fractures at fault-like shear zone tips and of any change in composition along strain gradients in the tonalites point to low fluid pressures and/or water-deficient conditions during the main ductile deformation event. In contrast, water-present conditions assisted deformation in the Sierra Nevada granites, where extensional veining is a dominant mode of displacement accommodation at the shear zone tips. However, if interpreted as a polyphase reactivation of the same structural planes, the veining and ductile fabric may also develop diachronously during decreasing temperature and increasing fluid activity (as occurs in the Lobbia area). Shear zones not associated with fluid-induced chemical changes have been described in other geologic environments during high temperature conditions (upper amphibolite/granulite facies to synmagmatic, e.g. Bhattacharyya and Hudleston, 2001; Arbaret and Burg, 2003), whereas greenschist facies mylonites are commonly accompanied by clear changes in major and trace element chemistry attributable to fluid–rock interaction (e.g. Tobish et al., 1991; Rolland et al., 2003).

The suggested change in the typology of foliation patterns at 'fault' termination as a function of T is not apparently supported by observations in the Lobbia area. Instead, ductile foliations at the tips of fault-like shear zones always develop asymmetrically around the pre-existing joint plane.

In general, joint planes appear well oriented with respect to the stress field of the overprinting ductile shearing phase as incipient strain-induced foliation is at 45° to the shear/joint plane. As a matter of fact, foliation (especially in weakly foliated tonalites) may be oriented at higher angles than 45° and up to nearly orthogonal but this reflects the disturbed stress field due to interaction between the joint planes during reactivation. The sinistral ductile shear reactivation and the prevalent right-stepped geometry of joints suggest that both brittle and ductile structures developed in a very similar kinematic regime and that joints may be precursory (in the sense of Crider and Peacock

(2004)) structures to ductile shear developing during progressive deformation.

7. Conclusions

The structural evolution of the Adamello tonalites recognized in the Lobbia outcrops is representative of high T solid state deformation in the early stages of subsolidus cooling of an intrusion emplaced at relatively shallow depth (ca. 10 km). In these outcrops, tonalites contain different types of ductile shear zones formed under amphibolite facies conditions ($T > 500$ °C), as determined based on the synkinematic mineral assemblage and the quartz CPO. The identical geochemical composition of undeformed and variably mylonitized tonalites indicates that no mass transfer occurred during ductile deformation. The characteristics of the ductile structures are determined by the geometric arrangement of a pervasive early (late-magmatic or early post-magmatic) set of precursor joints, locally intruded by pegmatite dykes and quartz veins. The dominant N–S precursor joints are typically discrete structures (with a length in the range of a few meters or tens of meters) arranged en-échelon, mainly forming right lateral steps with slightly overlapping terminations. These joints were reused as strongly localized discontinuous (fault-like) sinistral shear zones, with very minor deformation of the host tonalites away from their termination. The high displacement gradients established during slip along the fault-like segments resulted in the development of foliated domains on the contractional side of joint tips or at contractional jogs, with no opening of wing cracks in the opposite quadrants, consistent with fluid-deficient conditions. During increasing deformation, foliated domains at contractional jogs accommodate progressively higher shear strain due to synkinematic softening mechanisms and evolve into continuous shear zones connecting the tips of separate, fault-like, shear zones.

Acknowledgements

The MURST has supported this work. Reviews by Ron Vernon and Mark Swanson are gratefully acknowledged. The Geological Survey of the Provincia Autonoma di Trento provided invaluable helicopter facilities. Neil Mancktelow helped in reviewing an early version of the manuscript, with discussion, and with correction of the English. I thank Daria Pasqual for the XRF analyses, Karsten Kunze for the texture goniometer data, Luca Menegon for sample milling and Antonio Novello for the thin sections. Peter Christiansen kindly provided the original measurements of displacements in the shear zones of Sierra Nevada.

References

Arbaret, L., Burg, J.-P., 2003. Complex flow in lowest crustal, anastomosing mylonites: strain gradients in a Kohistan gabbro, northern Pakistan. Journal of Geophysical Research 108 (B10), 2467.

Austrheim, H., 1987. Eclogitization of lower crustal granulites by fluid migration through shear zones. Earth and Planetary Science Letters 81, 221–232.

Bhattacharyya, P., Hudleston, P., 2001. Strain in ductile shear zones in the Caledonides of northern Sweden: a three-dimensional puzzle. Journal of Structural Geology 23, 1549–1565.

Bianchi, A., Callegari, E., Jobstraibizer, P.G., 1970. I tipi petrografici fondamentali del plutone dell'Adamello (tonaliti, quarzodioriti, granodioriti e loro varietà leucocrate). Memorie dell'Istituto di Geologia e Mineralogia dell'Università di Padova 27, 1–148.

Bouchez, J.-L., Delas, C., Gleizes, G., Nedelec, A., Cuney, M., 1992. Submagmatic microfractures in granites. Geology 20, 35–38.

Boundy, T.M., Fountain, D.M., Austrheim, H., 1992. Structural development and petrofabric of eclogite facies shear zones, Bergen Arcs, western Norway: implications for deep crustal deformation processes. Journal of Metamorphic Geology 10, 127–146.

Bürgmann, R., Pollard, D.D., 1992. Influence of the state of stress on the brittle–ductile transition in granitic rock: evidence from fault steps in the Sierra Nevada, California. Geology 20, 645–648.

Bürgmann, R., Pollard, D.D., 1994. Strain accommodation about strike-slip fault discontinuities in granitic rocks under brittle-to-ductile conditions. Journal of Structural Geology 16, 1655–1674.

Christiansen, P.P., Pollard, D.D., 1997. Nucleation, growth and structural development of mylonitic shear zones in granitic rocks. Journal of Structural Geology 19, 1159–1172.

Connolly, P., Cosgrove, J., 1999a. Prediction of static and dynamic fluid pathways within and around dilational jogs, in: McCaffrey, K.J.W., Lonergan, L., Wilkinson, J.J. (Eds.), Fractures, Fluid Flow and Mineralization Geological Society of London, Special Publication, 155, pp. 105–121.

Connolly, P., Cosgrove, J., 1999b. Prediction of fracture-induced permeability and fluid flow in the crust using experimental stress data. American Association of Petroleum Geologists Bulletin 83, 757–777.

Crider, J.G., Peacock, D.C.P., 2004. Initiation of brittle faults in the upper crust: a review of field observations. Journal of Structural Geology 26, 691–707.

Del Moro, A., Pardini, G., Quercioli, C., Villa, I.M., Callegari, E., 1983. Rb/Sr and K/Ar chronology of Adamello granitoids, Southern Alps. Memorie della Società Geologica Italiana 26, 285–299.

Di Toro, G., Pennacchioni, G., 2004. Superheated friction-induced melts in zoned pseudotachylytes within the Adamello tonalites (Italian Southern Alps). Journal of Structural Geology 26, 1783–1801.

Di Toro, G., Pennacchioni, G., in press. Fault plane processes and mesoscopic structure of a strong-type seismogenic fault in tonalites (Adamello batholith, Southern Alps). Tectonophysics, in press.

Grant, J.A., 1986. The isocon diagram—a simple solution to Gresens' equation for metasomatic alteration. Economic Geology 81, 1976–1982.

Guermani, A., Pennacchioni, G., 1998. Brittle precursors of plastic deformation in a granite: an example from the Mont Blanc massif (Helvetic, western Alps). Journal of Structural Geology 20, 135–148.

Hansmann, W., Oberli, F., 1991. Zircon inheritance in an igneous rock suite from the southern Adamello batholith (Italian Alps). Contribution of Mineralogy and Petrology 107, 501–518.

Hobbs, B.E., Mühlhaus, H.-B., Ord, A., 1990. Instability, softening and localization of deformation, in: Knipe, R.J., Rutter, E.H. (Eds.), Deformation Mechanisms, Rheology and Tectonics Geological Society of London, Special Publication, 54, pp. 143–165.

Mancktelow, N.S., 1987. Quartz textures from the Simplon Fault Zone, southwest Switzerland and north Italy. Tectonophysics 135, 133–153.

Mancktelow, N.S., 2002. Finite-element modelling of shear zone development in viscoelastic materials and its implications for localization of partial melting. Journal of Structural Geology 24, 1045–1053.

Mancktelow, N.S., Pennacchioni, G., 2004. Microstructures of quartz mylonites: the importance of grain boundary fluids. Journal of Structural Geology 26, 47–69.

Mancktelow, N.S., Pennacchioni, G., in press. The control of precursor brittle fracture and fluid/rock interaction on the development of single and paired ductile shear zones. Journal of Structural Geology.

Martel, S.J., Pollard, D.D., Segall, P., 1988. Development of simple strike-slip fault zones, Mount Abbot quadrangle, Sierra Nevada, California. Geological Society of America Bulletin 100, 1451–1465.

Nemčok, M., Henk, A., Gayer, R.A., Vandycke, S., Hathaway, T.M., 2002. Strike-slip fault bridge fluid pumping mechanism: insights from field-based palaeostress analysis and numerical modelling. Journal of Structural Geology 24, 1885–1901.

Pennacchioni, G., 1996. Progressive eclogitization under fluid-present conditions of prealpine mafic granulites in the Austroalpine Mt. Emilius Klippe (Italian Western Alps). Journal of Structural Geology 18, 549–561.

Ramsay, J.G., Allison, I., 1979. Structural analysis of shear zones in an alpinised Hercynian granite (Maggia Lappen, Pennine Zone, Central Alps). Schweizerische Mineralogische und Petrographische Mitteilungen 59, 251–279.

Riklin, K., 1985. Contact metamorphism of Permian "red sandstones" in the Adamello area. Memorie della Società Geologica Italiana 26, 159–169.

Rolland, Y., Cox, S., Boullier, A.-M., Pennacchioni, G., Mancktelow, N., 2003. Rare earth and trace element mobility in mid-crustal shear zones: insights from the Mont Blanc Massif (Western Alps). Earth and Planetary Science Letters 214, 203–219.

Schmid, S.M., Casey, M., 1986. Complete fabric analysis of some commonly observed quartz c-axis patterns. Geophysical Monograph 36, 263–286.

Segall, P., 1998. Strike-slip shear zone in granodiorite, in: Snoke, A., Tullis, J., Todd, V. (Eds.), Fault-Related Rocks: A Photographic Atlas. Princeton University Press, pp. 146–151.

Segall, P., Pollard, D.D., 1983. Nucleation and growth of strike slip faults in granite. Journal of Geophysical Research 88, 555–568.

Segall, P., Simpson, C., 1986. Nucleation of ductile shear zones on dilatant fractures. Geology 14, 56–59.

Stipp, M., Tullis, J., 2003. The recrystallized grain size piezometer for quartz. Geophysical Research Letters 30.

Stipp, M., Stünitz, H., Heilbronner, R., Schmid, S., 2002. The eastern Tonale fault zone: a 'natural laboratory' for crystal plastic deformation of quartz over a temperature range from 250 to 700 °C. Journal of Structural Geology 24, 1861–1884.

Stipp, M., Fügenschuh, B., Gromet, L.P., Stünitz, H., Schmid, S.M., 2004. Contemporaneous plutonism and strike-slip faulting: a case study from the Tonale fault zone north of the Adamello pluton (Italian Alps). Tectonics 23.

Takagi, H., Goto, K., Shigematsu, N., 2000. Ultramylonite bands derived from cataclasite and pseudotachylyte in granites, northeast Japan. Journal of Structural Geology 22, 1325–1340.

Tobish, O.T., Barton, M.D., Vernon, R.H., Paterson, S.R., 1991. Fluid-enhanced deformation: transformation of granitoids to banded mylonites, western Sierra Nevada, California, and Southeastern Australia. Journal of Structural Geology 13, 1137–1156.

Tourigny, G., Tremblay, A., 1997. Origin and incremental evolution of brittle/ductile shear zones in granitic rocks: natural examples from the southern Abitibi Belt. Canada. Journal of Structural Geology 19, 15–27.

Tribe, I.R., D'Lemos, R.S., 1996. Significance of a hiatus in down-temperature fabric development within syn-tectonic quartz diorite complexes, Channel Islands, UK. Journal of the Geological Society of London 153, 127–138.

Tsurumi, J., Hosonuma, H., Kanagawa, K., 2003. Strain localization due to positive feedback of deformation and myrmekite-forming reaction in granite and aplite mylonites along the Hatagawa Shear Zone of NE Japan. Journal of Structural Geology 25, 557–574.

Urai, J.L., Means, W.D., Lister, G.S., 1986. Dynamic recrystallization of minerals, in: Heard, H.C., Hobbs, B.E. (Eds.), Mineral and Rock Deformation: Laboratory Studies—The Paterson Volume American Geophysical Union, Geophysical Monograph, 36, pp. 161–199.

Vernon, R.H., Johnson, S.E., Melis, E.A., 2004. Emplacement-related microstructures in the margin of a deformed pluton: the San José tonalite, Baja California, México. Journal of Structural Geology 26, 1867–1884.

Viola, G., Mancktelow, N.S., Seward, D., Meier, A., Martin, S., 2003. The Pejo fault system: an example of multiple tectonic activity in the Italian Eastern Alps. Geological Society of America Bulletin 115, 515–532.

Werling, E., 1992. Tonale-, Pejo- und Judicarien-Linie: Kinematik, Mikrostrukturen und Metamorphose von Tectoniten aus räumlich interferierenden aber verschiedenaltrigen Verwerfungszonen. PhD thesis, ETH Zürich, 276pp.

Wirth, R., Voll, G., 1987. Cellular intergrowth between quartz and sodium-rich plagioclase (myrmekite)—an analogue of discontinuous precipitation in metal alloys. Journal of Material Science 22, 1913–1918.